Construction and Building Materials 497 (2025) 143933

Contents lists available at ScienceDirect

Construction and Building Materials

journal homepage: www.elsevier.com/locate/conbuildmat

Electromechanical and piezoresistive behaviour of hydraulic lime mortar incorporating carbon microfibers for self-sensing applications

Ali Dalalbashi [a,1,*], Virginia Mendizabal [b,2], Anastasios Drougkas [c,3], Vasilis Sarhosis [a,4]

[a] School of Civil Engineering, University of Leeds, †Leeds, United Kingdom
[b] Department of Strength of Materials and Structural Engineering, Universitat Politècnica de Catalunya, Terrassa, Spain
[c] Department of Civil Engineering Educators, School of Pedagogical and Technological Education, Athens, Greece

ARTICLE INFO

Keywords:
Smart mortar
Self-sensing mortar
Hydraulic lime mortar
Piezoresistive
Carbon microfiber (CMF)
Silica fume

ABSTRACT

Self-sensing mortars, a type of smart material capable of monitoring structural behaviour under mechanical loading, have recently attracted significant attention. Although most research in this area has focused on cement-based systems, lime-based mortars remain relatively underexplored despite their importance in sustainable construction and heritage preservation. This study investigates the impact of carbon microfibers (CMFs) as a functional filler on the mechanical, electrical, and piezoresistive properties of hydraulic lime-based mortars. Mortar and paste mixes were prepared with different dosages of CMF (0 %, 0.05 %, 0.1 %, and 0.2 % by weight of the binder), both with and without silica fume as a pozzolanic additive. Mechanical tests, including flexural and compressive strength, as well as electrical resistivity measurements and electromechanical (piezoresistivity) evaluations, were performed. The results show that while silica fume enhances compressive strength, it tends to lower flexural strength, likely due to increased brittleness. The addition of CMF exhibited a nonlinear influence on the mechanical properties of the mixes, with strength decreasing up to 0.1 % CMF, followed by a slight increase at 0.2 % CMF. Similarly, the electrical properties (particularly piezoresistivity) also followed a nonlinear trend, showing enhanced sensitivity up to 0.1 % CMF and a reduction beyond that point. These trends suggest the presence of a percolation threshold around 0.1 % CMF The piezoresistive performance, assessed through gauge factor and linearity, also reached its peak at this dosage. The formulation of 0.1 % conductive material mixed with silica fume achieved a gauge factor of 311, which is 34 % higher than the mix containing 0.0 % CMF. This mix also displayed a coefficient of determination (R^2) of 0.97. In contrast, the mix without silica fume attained a gauge factor of 339, representing a 79 % increase compared to the mix with 0.0 % CMF, with an R^2 of 0.94. These results confirm that the sensing response was stable and highly reliable. Overall, 0.1 % CMF was identified as the optimal amount for improving the self-sensing behaviour of lime-based mortars. These findings confirm that CMF can effectively enhance the electromechanical response of traditional lime matrices without compromising their structural performance or their suitability for heritage materials.

1. Introduction

Self-sensing mortars, a category of smart materials, are increasingly recognised for their potential in structural health monitoring (SHM) of buildings and civil infrastructure [1]. Usually made using a cementitious matrix, these materials can detect mechanical strain and damage by registering changes in their electrical properties through a constitutive relation between strain and electrical resistivity known as piezoresistivity [2]. This is achieved by adding electrically conductive fillers that enhance electrical conductivity and form conductive networks that respond to mechanical deformation. As a result, such materials can detect strain and deformation in real-time, eliminating the need for

* Corresponding author.
E-mail addresses: a.dalalbashiesfahani@leeds.ac.uk (A. Dalalbashi), virginia.dolores.mendizabal@upc.edu (V. Mendizabal), adrougkas@civil.aspete.gr (A. Drougkas), v.sarhosis@leeds.ac.uk (V. Sarhosis).
[1] https://orcid.org/0000-0003-0486-1433
[2] https://orcid.org/0000-0003-0919-801X
[3] http://orcid.org/0000-0002-8647-9993
[4] http://orcid.org/ 0000-0002-5748-7679

https://doi.org/10.1016/j.conbuildmat.2025.143933
Received 16 July 2025; Received in revised form 3 September 2025; Accepted 3 October 2025
Available online 7 October 2025

external sensors [3].

Common conductive fillers include carbon nanotubes (CNTs), graphene (G), carbon black (CB), graphene nanoflakes (GNFs), and carbon microfibres (CMFs) [4–9]. Among these, CMFs have attracted particular interest due to their ability to enhance the self-sensing performance of mortars by improving strain sensitivity, facilitating electrical percolation, and contributing to mechanical strength, while not requiring chemical surfactants or sonication for dispersion in an aqueous solution [10,11]. Their relatively high aspect ratio enables effective conductivity at lower concentrations compared to graphite-based fillers, thereby reducing dispersion challenges. When combined with other fillers such as graphite or carbon nanotubes (CNTs), CMFs have shown remarkably high gauge factors. The gauge factor, defined as the relative change in electrical resistivity per unit of mechanical strain, reflects the material's sensitivity to strain. In some instances, these combinations have achieved gauge factors exceeding 100, with optimal performance usually observed at around 0.05 % by weight of the cement binder [6,12]. This results in distinct and reversible changes in electrical resistivity under mechanical loading, making CMFs particularly suitable for structural health monitoring applications. In contrast, alternatives like graphene nanoplatelets typically require higher dosages to attain comparable conductivity, which may adversely affect mechanical performance and increase material costs [13].

The piezoresistive response of cement-based self-sensing composites depends on both filler-related features and external factors. Among the intrinsic parameters, the type, size, dosage, and dispersion of conductive fillers are vital for forming a stable conductive network within the matrix [14–17]. An ideal filler content is necessary to balance conductive and non-conductive phases: too low a dosage makes the composite behave like conventional mortar or concrete with high resistivity, while excessive amounts can lead to poor dispersion, clustering, and increased porosity, which impair conductivity [14–17]. In addition to filler properties, piezoresistive behaviour is affected by raw materials, fabrication methods, and the applied loading regime. Environmental conditions are equally significant. For example, moisture content can enhance electrical conductivity by improving ionic transport, but too much moisture may reduce strain sensitivity depending on the type and amount of filler [18]. Similarly, curing age and temperature changes can impact resistivity by influencing pore structure and ion mobility. Nonetheless, the piezoresistive response generally remains linear and repeatable over a practical range of environmental conditions, highlighting its potential for structural health monitoring applications [19–21].

Beyond material composition, recent advances in structural health monitoring (SHM) demonstrate that techniques such as acoustic emission, digital image correlation, and piezoelectric sensing are effective for detecting crack initiation, identifying fracture modes, and tracking crack propagation in cementitious composites [22,23]. The use of piezoelectric and fibre-reinforced sensor networks in real structures further showcases the practical potential of SHM systems under various service conditions [8]. These developments highlight promising pathways for expanding self-sensing technology to hydraulic lime mortars, reinforcing the relevance of the present study.

Most studies have focused on cement-based composites, while lime-based mortars (commonly used in heritage restoration and sustainable building practices) have received comparatively less attention regarding their self-sensing capabilities. Research has shown that the addition of 0.15 % CNTs reduces the electrical resistivity of lime-based pastes by 12 % [24]. Additionally, adding 2.5 % graphite and 0.1 % CMF to low-strength lime-based mortar (with compressive strength less than 1.5 MPa) not only decreases the electrical resistivity (by 50 % and 70 %, respectively) but can also slightly improve its flexural and compressive strength [25,26]. Low-strength mortars are mainly used in heritage conservation, where compatibility and flexibility are more important than load-bearing capacity. Conversely, high-strength hydraulic lime mortars, especially when enhanced with silica fume, are vital for modern uses that demand durability and structural integrity, such as strengthening and retrofitting. Despite their practical significance, high-strength self-sensing lime mortars are still largely unexplored, and their piezoresistive behaviour remains poorly understood.

Lime binders in construction are mainly classified into two types: non-hydraulic (aerial or high calcium) lime and hydraulic lime. Non-hydraulic lime, mainly made of calcium hydroxide, $Ca(OH)_2$, sets through carbonation as it reacts with atmospheric carbon dioxide (CO_2). Hydraulic lime, however, contains reactive components such as dicalcium silicate, Ca_2SiO_4, enabling it to set by both hydration and carbonation [27]. The initial setting of hydraulic lime mortars occurs when calcium silicate hydrate (C-S-H) compounds form, followed by the gradual carbonation of the remaining calcium hydroxide. This secondary carbonation helps seal pores and microcracks, limiting further CO_2 ingress and improving long-term durability [28]. Lime-based mortars are extensively used in masonry buildings and the restoration of historic structures because they are compatible with traditional materials. Their breathability, chemical affinity, and ability to accommodate structural movements make them especially suitable for conservation projects on heritage structures. Unlike modern cement mortars, which tend to be rigid and less compatible, lime mortars have a lower modulus of elasticity and higher porosity. These characteristics allow them to dissipate internal stresses and promote moisture evaporation, reducing the risk of water trapping and material deterioration [29–31]. These microstructural and mechanical differences also influence their self-sensing behaviour. Cement-based systems rely on dense C-S-H phases that stabilise fibre-based conductive pathways [32], whereas lime mortars, with higher porosity and dual hydration-carbonation reactions, allow ionic conduction but form less stable conductive networks. Their increased deformability further improves strain transfer to fillers, which may boost sensitivity but reduce stability. These differences emphasise the need for targeted research on self-sensing lime mortars.

This study aims to bridge the existing knowledge gap by systematically investigating the effect of carbon microfiber (CMF) dosage on the mechanical, physical, and piezoresistive properties of high-strength hydraulic lime-based mortars and pastes. This area has received very limited attention compared to cement-based systems or low-strength lime mortars. The developed mixture will be used for strengthening masonry structures, especially as matrix components in textile-reinforced mortar (TRM) composites. CMF contents of 0 %, 0.05 %, 0.1 %, and 0.2 % (by binder weight) are evaluated herein. Additionally, silica fume is incorporated into selected mixes to assess the impact of pozzolanic reactions on matrix performance. The materials are subjected to a comprehensive testing program, including assessments of bulk density development, flexural and compressive strength, elastic modulus, electrical resistivity, and piezoresistivity. The novelty of this research lies in demonstrating, for the first time, how the combined use of CMFs and silica fume can be customised to produce multifunctional hydraulic lime-based composites that deliver both enhanced mechanical reinforcement and real-time damage detection. Such multifunctional performance is essential in heritage preservation and reinforcement, where materials must stay compatible with historic masonry while enabling non-intrusive monitoring of damage and durability. The findings aim to support the development of advanced lime-based smart composites for repair and strengthening heritage structures but also for constructing modern masonry structures.

2. Experimental program

2.1. Overall test description

The experimental campaign included a comprehensive programme of material characterisation, including mechanical testing, electrical resistivity measurements, and electromechanical tests on natural hydraulic lime-based mortar and paste. The following sections describes in detail the raw materials, specimen preparation procedures, and test methods employed. An overview of the experimental programme is provided in Fig. 1 to facilitate clarity and coherence in presenting methodology.

2.2. Materials

Eminently hydraulic natural hydraulic lime (NHL 5.0) and silica fume powder (average particle size of 0.1–1 μm), based on EN 459–1 [33] and EN 13263–1 [34], respectively, were used as binders. NHL 5.0 was selected over the more common, moderately hydraulic NHL 3.5 to meet the anticipated higher mechanical demands on the material. In addition, the aggregate used in this study was CEN standard sand, EN 196–1 [35], characterised by a nominal grain size distribution of 0–2 mm, which is suitable for plaster mortar and intervention mortar. All materials were manufactured and supplied by the manufacturer in accordance with the relevant standards. Chopped carbon microfibers (CMFs) were used as a functional filler. The CMFs were coated with a glycerine-based sizing agent, making them compatible with water-based systems. The CMFs had a length of 6 mm, a tensile strength of 4 GPa, strain of 1.7 %, and an elastic modulus of 240 GPa. Table 1 reports the physical properties of CMFs. The CMFs were incorporated in various proportions as a percentage of the binder's weight. They were used in amounts of 0.05 %, 0.1 %, and 0.2 % of binder weight, based on [25,26].

The mortar mixing process adhered to the EN 196–1 [35], with the binder and aggregate proportioned by weight in a 1:3 ratio. Silica fume was incorporated at 5 % of the total binder weight as a replacement for NHL 5.0. The water-to-binder (w/b) ratio was determined based on the Vicat consistency test [36] and the required workability for plaster applications, which will be discussed later. The mixing procedure was as follows: First, CMFs were dispersed in water and mixed for one minute to ensure uniform distribution, based on [25]. Next, the binder was gradually added to the liquid and mixed slowly for five minutes. Finally, the aggregate was introduced to the paste and mixed for an additional five minutes at a slow mixing speed.

Fresh mortar was poured into steel moulds, compacted with a tamper rod, and covered with a plastic sheet for seven days to prevent moisture loss. After the initial seven days, the plastic was removed, and the specimens were stored in laboratory conditions (20°C and 60 % RH) for an additional 53 days. All specimens were demoulded after two days.

To investigate the effects of aggregates and silica fume on the electrical properties of the self-sensing mortar, it was decided that mortar without silica fume and binder paste without aggregates to be produced. The binder pastes were prepared and cured using a similar mixing process to that of the mortar, excluding the addition of the aggregate.

The specimens tested were identified using the notation X-Y-Z, where X indicates the type of binder (SF for mixes containing silica fume while NSF for mixes without silica fume), Y denotes the mix type (M for mortar and P for paste). Z shows the dosage of carbon microfibers (CMF), expressed as a percentage of the binder weight (0 %, 0.05 %, 0.1 %, and 0.2 %). For instance, the specimen labelled SF-M-0.1 represents a mortar mix that includes silica fume and 0.1 % CMF. A comprehensive list of all

Table 1
Physical properties of CMFs.

Density [g/cm^3]	Filament diameter [μm]	Single filament resistivity [μ Ω m]
1.8	7	15

Table 2
List of the different mortar and paste mixes considered in this study.

Mix	NHL 5.0	Silica fume	Sand	CMF [%]
SF-M−0	✓	✓	✓	0.00
SF-M−0.05	✓	✓	✓	0.05
SF-M−0.1	✓	✓	✓	0.10
SF-M−0.2	✓	✓	✓	0.20
SF-P−0	✓	✓	×	0.00
SF-P−0.05	✓	✓	×	0.05
SF-P−0.1	✓	✓	×	0.10
SF-P−0.2	✓	✓	×	0.20
NSF-M−0	✓	×	✓	0.00
NSF -M−0.05	✓	×	✓	0.05
NSF-M−0.1	✓	×	✓	0.10
NSF-M−0.2	✓	×	✓	0.20
NSF-P−0	✓	×	×	0.00
NSF-P−0.05	✓	×	×	0.05
NSF-P−0.1	✓	×	×	0.10
NSF-P−0.2	✓	×	×	0.20

✓: Component included in the mix; × : Component not included in the mix. aggregates/binder: 3/1, w/b: 0.65, silica fume 5 % of the total binder weight as a replacement for NHL 5.0

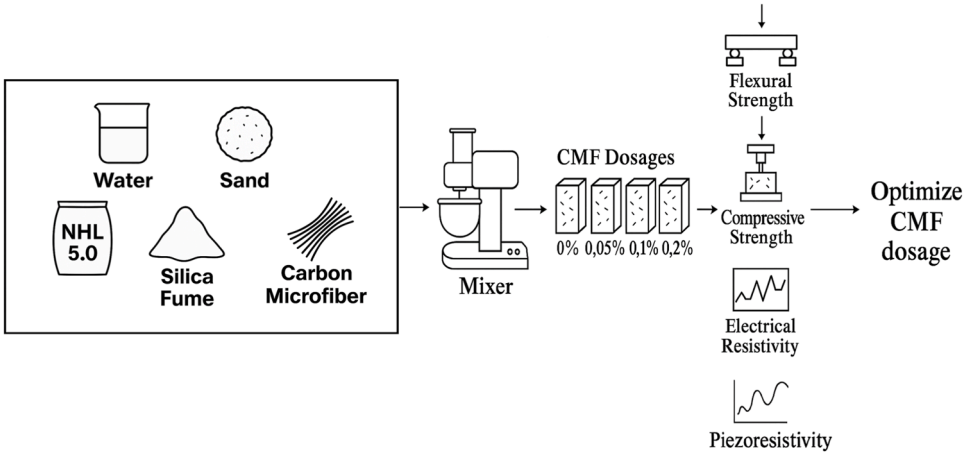

Fig. 1. Overview of the experimental program.

mortar and paste formulations undertaken in this study is presented in Table 2.

2.3. Material characterisation tests

The Vicat consistency test was conducted to determine the optimal w/b ratio required to achieve the standard consistency for fresh mortar, as specified in EN 196–3 [35]. The aim was to establish an appropriate w/b ratio while considering the potential decreased workability resulting from the addition of CMFs. To accommodate this effect, the target penetration depth was modified to 10 ± 1 mm, rather than the 6 ± 2 mm recommended by the standard [35]. This decision was influenced by the functional requirements of using the developed mortar as a matrix in textile-reinforced mortar (TRM) composites intended for masonry strengthening, which is the intended application of the material. In TRM systems, high workability is essential to ensure proper impregnation of the textile, effective mechanical interlocking, and strong adhesion between the mortar and reinforcement [37,38]. To assess the impact of different w/b ratios, tests were conducted using ratios of 0.55, 0.65, and 0.75, which produced penetration depths of 37 mm, 9 mm, and 3 mm, respectively. Based on these results, and considering the target penetration depth of 10 ± 1 mm, a w/b ratio of 0.65 was chosen for all mixes.

The flexural and compressive strengths of the mortars were evaluated in accordance with EN 1015–11 [39]. Three prismatic specimens (40 × 40 × 160 mm³) were prepared for each mix to determine the flexural strength. The flexural tests were conducted using a three-point bending test setup, with a span of 100 mm between supports. Following the flexural tests, the two halves of each specimen were subjected to compression testing to assess their compressive strength. All tests were conducted using an MTS machine (Exceed Electromechanical Test System: E45) under load-controlled conditions, with loading rates of 10 N/s for flexural tests and 50 N/s for compressive tests.

The elastic modulus of the mortar mixes was determined using cube specimens (50 × 50 × 50 mm³), based on [25]. For each mix, three specimens were prepared, and their deformations were measured using two linear strain gauges, each with a gauge length of 20 mm. Additionally, the density of the cubes was monitored throughout the curing process at 7, 28, and 60 days to assess their curing over time.

The electrical resistivity of the specimens was evaluated using cube

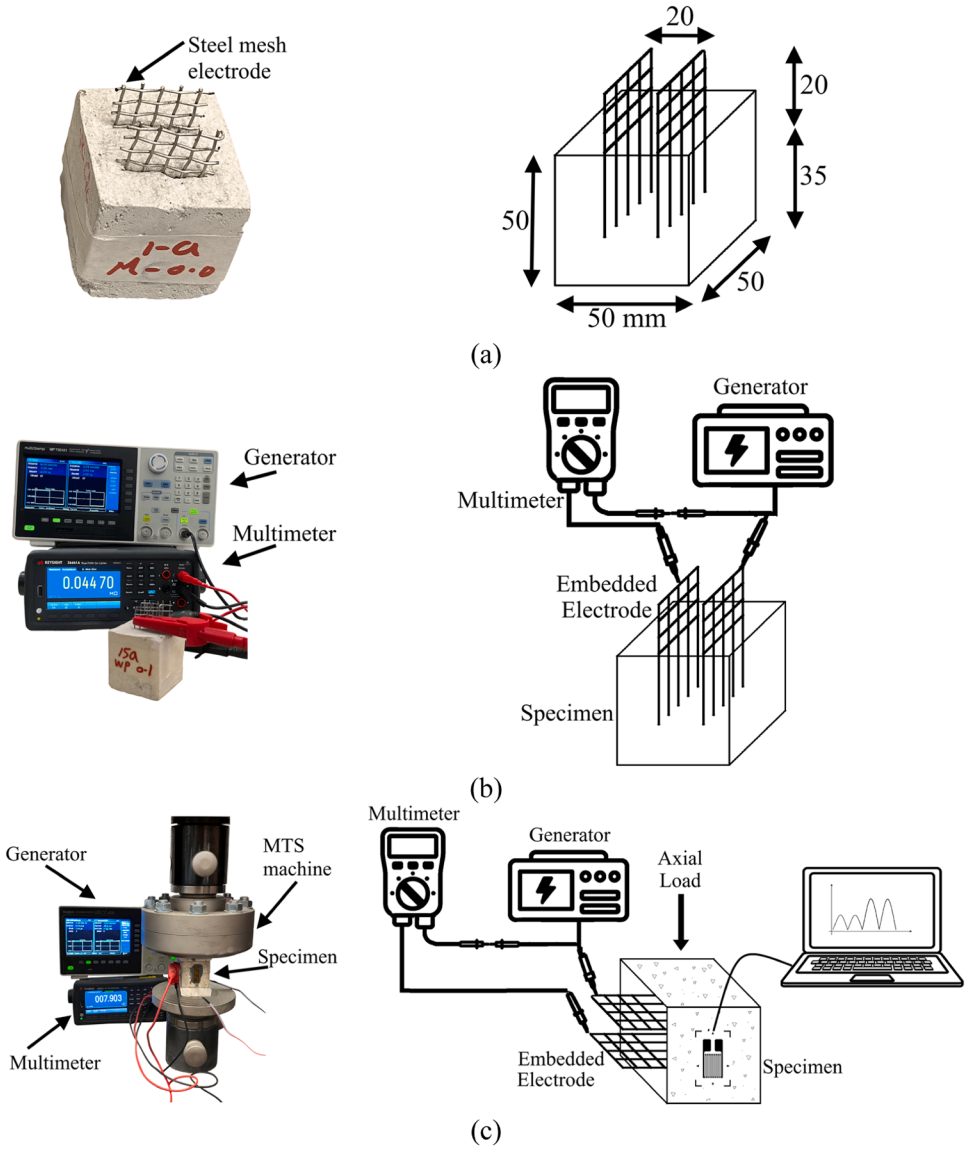

Fig. 2. (a) Arrangement of embedded electrodes; (b) Electrical resistivity setup; (c) Piezoresistivity setup.

samples measuring 50 × 50 × 50 mm^3 , following the procedure outlined in [25]. Each specimen was fitted with steel mesh electrodes that measured 55 mm in length and 30 mm in width, which were embedded 35 mm into the specimen, as illustrated in Fig. 2a. The distance between the steel meshes was 20 mm. Electrical resistivity measurements were performed at 7, 28, and 60 days of curing. A function generator (MP750510) produced a sine waveform with a frequency of 10 Hz and an amplitude range of ±500 mV (Fig. 2b). In addition, a multimeter (Keysight 34466 A) was used to measure the electrical resistance (R) of specimens.

The piezoresistivity of the mortar cube specimens (SF-M and NSF-M mixes) was evaluated through electromechanical testing, as described in [25]. Each test started with a base stress of 0.2 MPa, acting as a preload to guarantee even contact between the specimen and loading platens. From this baseline, the specimens were subjected to a cyclic compression load with increasing magnitude while continuously monitoring changes in electrical resistivity and strain, as illustrated in Fig. 3. Each cycle was repeated twice, with target stress levels of 0.4, 0.8, and 1.2 MPa. These target stress values were determined as percentages of the compressive strength of the NSF-M-0 mix. At each target load, a constant load was maintained for 20 s. An MTS machine applied cyclic loads at 50 N/s, consistent with compressive strength test results. To measure specimen deformation, two linear strain gauges (each 20 mm in length) were affixed along the loading direction and placed at the centre of the specimens, as shown in Fig. 2c. In addition, electrical resistivity was measured during the piezoresistivity tests using the same two-probe setup and instrumentation described earlier. It should be noted that piezoresistivity was conducted solely on mortar mixes (SF-M and NSF-M).

The resistivity (ρ) of specimens was determined through the two-probe method according to Ohm's second law:

$$\rho = R\frac{A}{L} \tag{1}$$

where A represents the cross-sectional area of the specimen in the plane perpendicular to the measurement direction ($A = 2500\ mm^2$) and L denotes the distance between the probes along the measurement direction ($L = 20$ mm). The gauge factor, λ, which indicates the magnitude of the piezoresistive effect during mechanical loading, was determined as follows [25]:

$$\lambda = \frac{\Delta\rho}{\rho}\varepsilon \tag{2}$$

where $\Delta\rho/\rho$ is the relative change in resistivity and ε is the axial strain of the specimen. A higher λ indicates greater sensitivity of the material's electrical resistivity to applied axial strain. Optimising the piezoresistive effect typically occurs near the percolation threshold. The concept of sensing linearity (δ) is introduced to evaluate the sensing performance, indicating the 95 % confidence interval for the predicted linear regression. This parameter quantifies the maximum deviation of the sensor's output from the regression line, which correlates resistivity with strain. Higher λ values and lower δ values signify better sensitivity and linearity of the smart sensor.

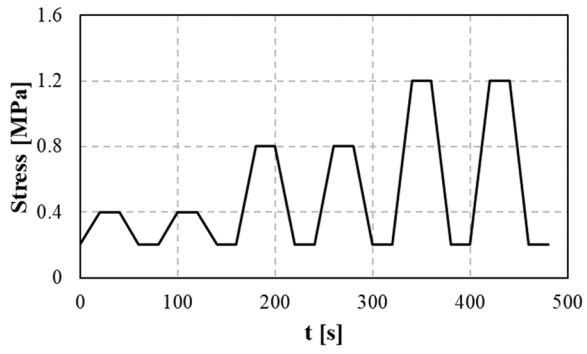

Fig. 3. Repeated compression loading pattern for characterising the piezoresistivity of mortar cubes.

3. Results and discussion

3.1. Physical and mechanical properties

Fig. 4 illustrates the average development of bulk density (ρ_b) for mortar and paste mixes over time for all mixes. All mixes exhibit an initial decline in density due to hydration and water evaporation. The change in slope around day 28 signifies the transition from hydration to carbonation, resulting in only minor increases in density thereafter [25,40]. Pastes exhibited a similar trend; however, densities (particularly in NSF-P) continued to decrease gradually, likely due to their finer pore structure impeding water loss. Moreover, the presence of fine aggregates significantly increases the bulk density of mortars compared to pastes, as aggregates occupy space more efficiently and decrease overall porosity, which explains the consistently higher densities observed in mortar mixes. Table 3 also presents the mean bulk density of all mixes at 60 days. Mortars incorporating silica fume (SF-M) exhibited consistently lower bulk densities compared to mortar mixes without silica fume (NSF-M). At 0 % CMF, NSF-M-0 had a bulk density of 1931 Kg/m^3 , while the silicon fume mix (SF-M-0) recorded a density of 1900 Kg/m^3 , indicating a 1.6 % decrease. At CMF content of 0.05 %, 0.1 %, and 0.2 %, the bulk density of SF-M mixes relative to NSF-M mixes decreased by approximately 2.5 %, 2.9 %, and 2.8 %, respectively. Furthermore, increasing the CMF content caused a decrease in the bulk density of the mixes. For the SF-M series, the bulk density declined by 1.8 %, 2.9 %, and 2.8 % at CMF levels of 0.05 %, 0.1 %, and 0.2 %, respectively, compared to the SF-M-0 mix. In the NSF-M series, the respective reductions were 0.9 %, 1.7 %, and 1.6 %. These results indicate that CMF reduces bulk density across all mixes, with the most significant decrease observed at a 0.1 % CMF level. Moreover, the presence of silica fume appears to enhance CMF's effect, making the matrix more responsive to fibre content. This is likely due to the combined impact of finer particle size and decreased workability, which may increase air entrapment and micro-void formation during mixing. Further microstructural analysis is recommended to understand better and validate this behaviour [20,34] A similar trend appears in the paste mixes (SF-P and NSF-P), where bulk density decreases with the addition of silica fume and increasing CMF content. This consistent pattern across both mortar and paste formulations shows that the reduction in bulk density is mainly influenced by the presence of CMF and silica fume, rather than by including aggregates. Therefore, the observed reductions are primarily affected by the fine particle characteristics and the mixing dynamics of the binder phase.

Fig. 5a, b and Table 3 present the average flexural and compressive strength values of mortar and paste mixes containing varying amounts of carbon microfibers (CMF). Overall, the results reveal a nonlinear relationship between CMF content and mechanical performance. In the SF-M mix, increasing the CMF content from 0 % to 0.1 % leads to a 25 % reduction in flexural strength, possibly due to poor fibre dispersion and/or increased porosity. However, further increasing the CMF content to 0.2 % results in a 27 % increase in flexural strength compared to the SF-M-0.1 mix. A similar trend is observed in compressive strength, with a 15 % decrease at 0.1 % CMF followed by a 15 % increase at 0.2 %. The mortar mixes without silica fume (NSF-M) exhibit similar behaviour. There is a 14 % reduction in flexural strength when the CMF increases from 0 % to 0.1 %. This is followed by a 25 % increase in flexural strength when the CMF rises from 0.1 % to 0.2 %. In terms of compressive strength, the changes are a 16 % decrease and a 10 % increase, respectively. In paste mixes, including SF-P and NSF-P, a similar

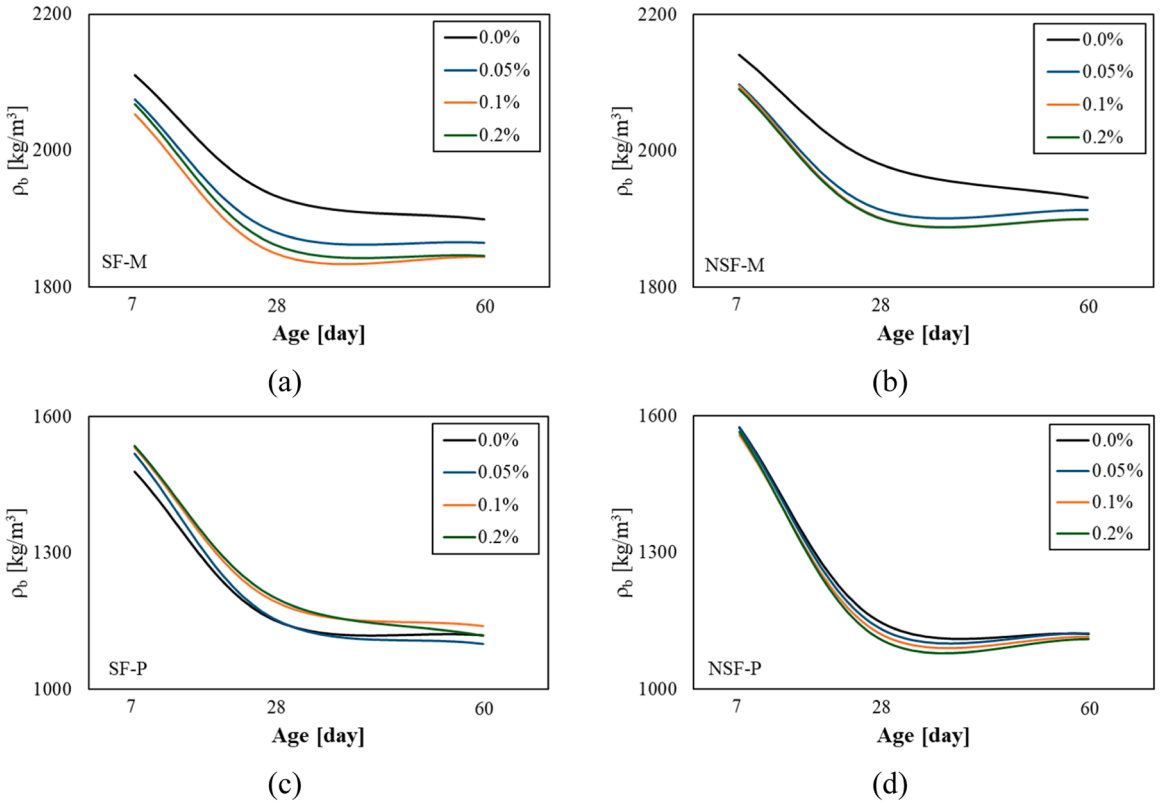

Fig. 4. Development of bulk density (ρ_b) of mixes: (a) SF-M; (b) NSF-M; (c) SF-P; (d) NSF-P.

Table 3
Physical and mechanical properties of mixes at 60 days of age*.

Mix	ρ_b [Kg/m^3]	f_b [MPa]	f_c [MPa]	E [MPa]	ρ [Ω.cm]	λ [-]	δ [-]
SF-M−0	1900 (1)	1.3 (16)	4.1 (4)	3950 (8)	8.0×10^6	204	9.9×10^{-5}
SF-M−0.05	1865 (1)	1.0 (3)	4.0 (6)	4580 (4)	7.2×10^6	295	8.3×10^{-5}
SF-M−0.1	1844 (1)	1.0 (5)	3.5 (5)	4730 (6)	5.2×10^6	311	6.9×10^{-5}
SF-M−0.2	1846 (0.2)	1.3 (1)	4.1 (3)	4310 (1)	5.8×10^6	250	1.0×10^{-4}
NSF-M−0	1931 (5)	1.4 (14)	3.6 (9)	5580 (4)	12.1×10^6	70	8.6×10^{-5}
NSF-M−0.05	1913 (1)	1.2 (6)	3. 6 (9)	6730 (11)	10.7×10^6	269	6.7×10^{-5}
NSF-M−0.1	1899 (0.2)	1.2 (8)	3.0 (6)	5460 (7)	7.8×10^6	339	6.1×10^{-5}
NSF-M−0.2	1900 (2)	1.5 (2)	3.3 (8)	4670 (6)	8.7×10^6	224	7.6×10^{-5}
SF-P−0	1120 (3)	1.0 (19)	3.3 (9)	-	2.9×10^6	-	-
SF-P−0.05	1099 (2)	0.6 (7)	3.4 (10)	-	1.6×10^6	-	-
SF-P−0.1	1090 (3)	1.0 (8)	3.0 (9)	-	1.5×10^6	-	-
SF-P−0.2	1091 (3)	1.2 (16)	3.2 (8)	-	1.4×10^6	-	-
NSF-P−0	1121 (1)	0.9 (8)	3.2 (13)	-	3.3×10^6	-	-
NSF-P−0.05	1118 (1)	0.8 (10)	3.5 (6)	-	1.7×10^6	-	-
NSF-P−0.1	1115 (0.4)	1.1 (9)	2.9 (8)	-	1.4×10^6	-	-
NSF-P−0.2	1109 (0.3)	1.4 (5)	3.0 (10)	-	1.5×10^6	-	-

ρ_b: Bulk density; f_b: Flexural strength; f_c: Compressive strength; E: Elastic modulus; ρ: Electrical resistivity; λ: Gauge factor; δ: sensing linearity.
* Coefficients of variation in percentage terms are provided inside parentheses.

observation is made. This behaviour may arise from a balance between fibre agglomeration at lower contents and enhanced fibre-matrix interaction at higher contents, as supported by previous studies [8,41].

Fig. 5c and Table 3 illustrate how the elastic modulus varies with different CMF dosages for both the SF-M and NSF-M mixes. The results demonstrate a nonlinear trend. The elastic modulus of SF-M mixes increases by 20 % with the addition of 0.1 % CMF compared to SF-M-0. However, at 0.2 % CMF content, the elastic modulus declines by 9 % compared to SF-M-0.1. For NSF-M mixes, the elastic modulus increases by 21 % with the addition of 0.05 % CMF but then shows a decreasing trend as the CMF content rises to 0.2 %. At this level, the elastic modulus decreases by 31 % compared to NSF-M-0.05. Although compressive

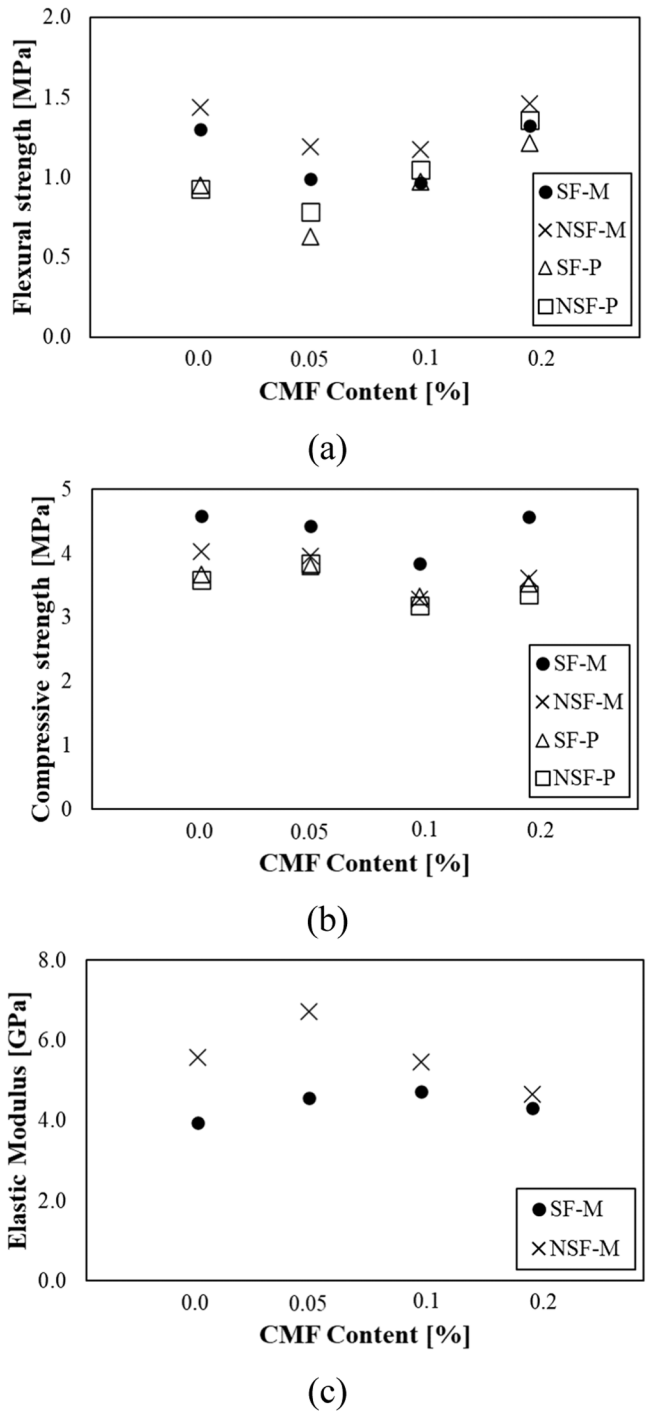

Fig. 5. Average mechanical properties of mixes: (a) flexural strength; (b) compressive strength; (c) elastic modulus.

strength and elastic modulus are usually related, this study shows divergence at higher fibre contents. This behaviour can be attributed to the differing micromechanical mechanisms that influence stiffness and strength. While the elastic modulus mainly depends on the integrity of the matrix and the intrinsic stiffness of the fibres, strength is more influenced by factors such as crack-bridging efficiency and the quality of the fibre-matrix interface [41]. At 0.2 % CMF, fibre clustering and increased porosity may disrupt matrix continuity, reducing stiffness despite gains in strength. In addition, the mixes without silica fume (NSF-M) consistently exhibit higher flexural strength and elastic modulus compared to those containing silica fume (SF-M), as presented in Table 3. This difference may be attributed to increased autogenous shrinkage, the development of micro-cracks, and the enhanced brittleness typically associated with the incorporation of silica fume [40]. However, this trend is reversed regarding compressive strength, where SF-M mixes demonstrate better performance than NSF-M. The improved compressive strength in SF-M is attributed to the pozzolanic activity of silica fume, which refines the pore structure and forms a denser matrix.

These findings regarding mechanical behaviour align with the observed trends in bulk density. The reductions in strength and stiffness at higher CMF contents correspond with increased porosity and decreased matrix compactness, as evidenced by lower bulk densities. A study [25] on self-sensing mortars using NHL 3.5 binder with CMF dosages from 0 % to 0.2 % showed that 0.01 % CMF improved flexural and compressive strength, while higher dosages reduced strength. Interestingly, the elastic modulus increased steadily with increasing CMF content. In contrast, the present study, which used NHL 5.0 as the binder, demonstrated an initial decrease in strength up to 0.1 % CMF, followed by partial recovery at 0.2 % CMF. This difference in behaviour can be linked to the inherent differences between the two binders. NHL 5.0 is denser and mechanically stronger than NHL 3.5. Also, NHL 5.0 has a more compact matrix that is more susceptible to disruption at low fibre contents when compared to NHL 3.5. However, at higher CMF dosages, the improved fibre bridging, and network formation can compensate for the early strength loss. Additionally, while lower CMF dosages may be sufficient to enhance performance in the more porous NHL 3.5 matrix, higher CMF contents seem necessary to interact effectively with the denser NHL 5.0 matrix.

3.2. *Electrical resistivity and piezoresistivity properties*

Fig. 6 and Fig. 7 illustrate the average evolution of electrical resistivity over time as a function of CMF content for all mixes. Additionally, Table 3 reports the mean electrical resistivity of all mixes at 60 days. In both SF-M and NSF-M mortar mixes, resistivity increases rapidly up to 28 days, after which the rate of growth slows, mirroring trends observed in bulk density development. In contrast, the paste mixes (SF-P and NSF-P) display a more gradual and consistent increase throughout the 60-day curing period. Notably, pastes without CMF exhibit a steeper rise in resistivity compared to those containing CMF, suggesting that the presence of fibres and associated increase in porosity slows down the development of electrical resistivity. The continuous pore network in paste specimens is sensitive to carbonation and moisture redistribution, which reduces ionic mobility over time and increases resistivity in 0 % CMF pastes. In contrast, aggregates in mortars disrupt pore connectivity, creating a stable microstructure that limits variability at later ages [42]. These results highlight the significant influence of aggregates and the pore network on the electrical resistivity of lime-based composites, in line with previous findings [25]. Furthermore, the influence of silica fume is clear in mortars, as its ultrafine particles enhance the pore structure and packing density, thus promoting conductive pathways and leading to lower resistivity in SF-M compared to NSF-M [43].

The effect of CMF content on electrical resistivity reveals a nonlinear trend, particularly in the mortar mixes, as shown in Fig. 7. As the CMF content increases from 0 % to 0.1 %, a notable decrease in resistivity is observed, followed by a modest increase at 0.2 %. For example, SF-M-0.1 exhibits a 35 % lower resistivity than SF-M-0, while SF-M-0.2 shows an 11 % increase relative to SF-M-0.1. Similarly, NSF-M mixes demonstrate a 36 % reduction in resistivity from 0 % to 0.1 % CMF, followed by a 12 % rise from 0.1 % to 0.2 %. These patterns suggest that small additions of CMF (up to 0.1 %) enhance electrical conductivity through improved fibre dispersion and network formation. However, at higher fibre contents, agglomerations and increased porosity may disrupt conductive pathways, resulting in a slight increase in resistivity, as supported by previous studies [8,25,41]. In the current study, this interpretation remains indirect because no SEM data have been collected. These findings are consistent with mechanical and bulk

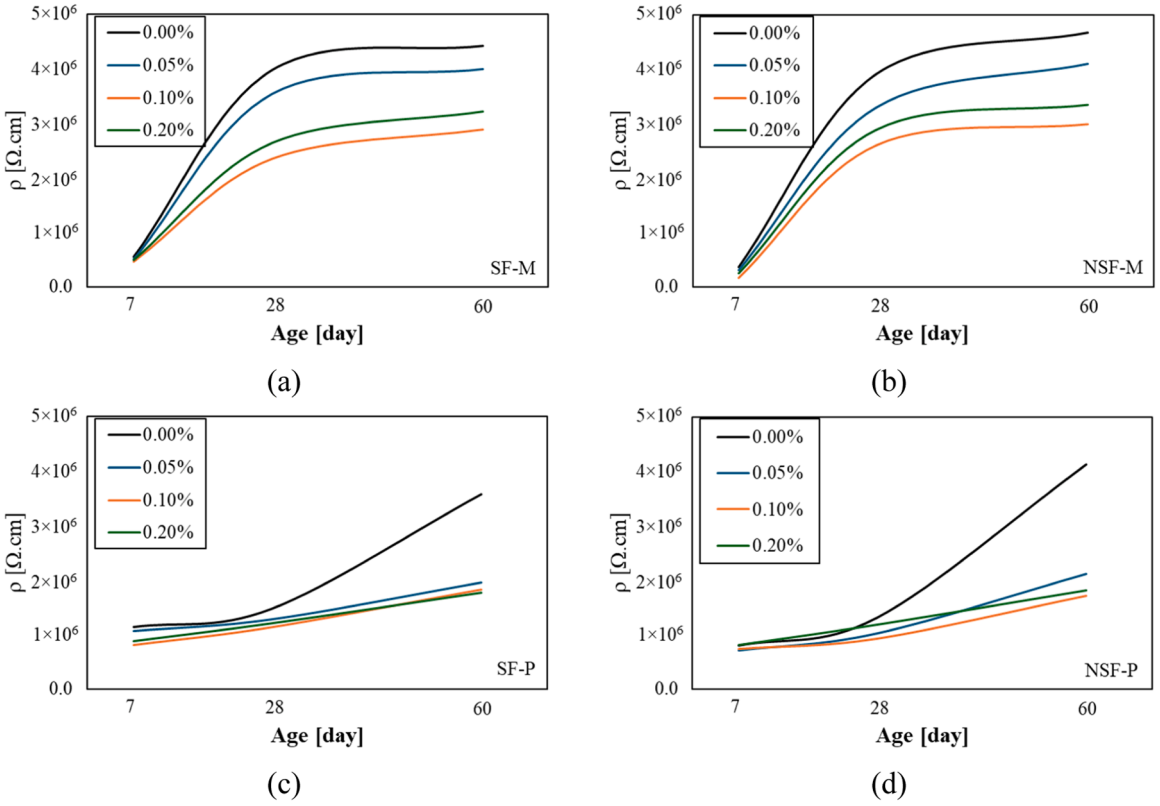

Fig. 6. Average development of resistivity (ρ) for the mixes: (a) SF-M; (b) NSF-M; (c) SF-P; (d) NSF-P.

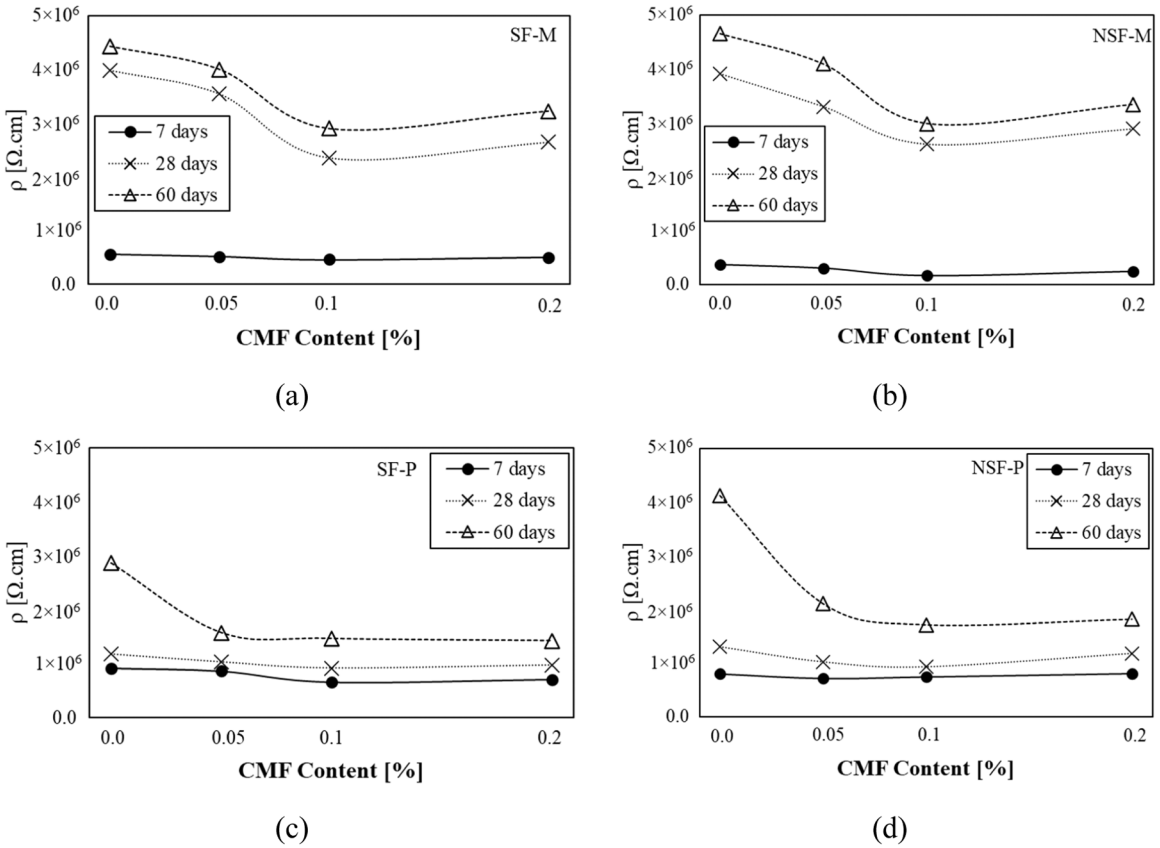

Fig. 7. Average evolution of resistivity as a function of CMF content at different curing ages: (a) SF-M; (b) NSF-M; (c) SF-P; (d) NSF-P.

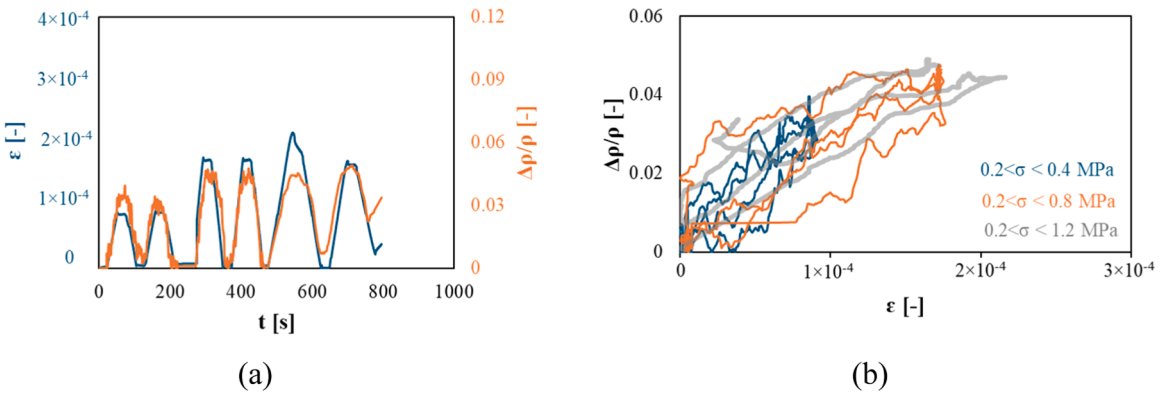

Fig. 8. Piezoresistive response of SF-M-0 mortar under cyclic loading: (a) time histories of axial strain (ε) and relative change in resistivity (Δρ/ρ); (b) correlation between axial strain and relative resistivity change at varying compressive stress ranges.

density results, where the lowest bulk density and elastic modulus at 0.2 % CMF indicate increased porosity and reduced matrix continuity, which also hinder electrical connectivity. Although direct porosity or microstructural data were not collected in this study, the observed resistivity trends, supported by bulk density and mechanical data, provide indirect evidence of the role of aggregates, silica fume, and CMFs in governing the conductive behaviour of lime-based composites. Future work will include porosity analyses to further validate these interpretations.

In the paste mixes, the influence of CMF content on resistivity is less pronounced. The most significant changes occur at 0 % CMF, where both SF-P and NSF-P exhibit the highest resistivity values. The introduction of 0.1 % CMF results in substantial reductions of 49 % and 58 % for SF-P and NSF-P, respectively. Beyond this threshold, resistivity remains relatively constant. This suggests that a small quantity of CMF significantly enhances conductivity by introducing effective conductive pathways, while further additions provide limited additional benefit. This effect is likely due to the absence of aggregates and the dominant role of pore structure in governing conductivity in paste systems.

Fig. 8 presents the piezoresistivity response of SF-M mortar under cyclic loading. in Fig. 8a, the time histories of axial strain (ε) and the relative change in electrical resistivity (Δρ/ρ) are compared, while Fig. 8b illustrates the correlation between axial strain and Δρ/ρ at different compressive stress level. The behaviour observed in all tested specimens was consistent with the representative trends illustrated in Fig. 8. Additional evidence is provided in Appendix Fig.AP. 1-to-4, which present representative results for one specimen from each mix type. The cyclic response demonstrates three key characteristics: (1) A linear and highly repeatable relationship between strain and resistivity during cyclic loading at 0.4 MPa and 0.8 MPa. (2) The onset of minor residual strain and a slight increase in hysteresis at a stress level of 1.2 MPa. (3) The maintenance of stable piezoresistive sensitivity, despite the appearance of stress-strain nonlinearities at higher stress levels. The apparent linearity observed below 0.8 MPa indicates that the material response is primarily driven by elastic deformation. In contrast, the behaviour at 1.2 MPa suggests the possibility of early-stage microstructural changes, particularly at the fibre-matrix interface, that require further investigation. In the 0 % CMF mix (e.g., SF-M-0 in Fig. 8b), the strain-resistivity relationship seems less distinct due to increased scatter, which aligns with a sub-percolation regime where the lack of conductive fibres results in greater variability caused by ionic conduction and electrode effects. Nevertheless, regression analysis (Appendix Fig.AP. 1-to-4) indicates that all cases still show R^2 values above 0.90, confirming that despite the visible scatter, the fundamental relationship remains strongly linear.

Fig. 9 and Table 3 present the mean values of gauge factor (λ) and sensing linearity (δ) for mortar mixes with varying amounts of CMF. For both SF-M and NSF-M mixes, the gauge factor exhibits a nonlinear relationship with CMF content. Specifically, as CMF content increases from 0 % to 0.1 %, λ also increases, reaching its peak at 0.1 %. However, a further increase to 0.2 % results in a reduction in λ. In contrast, δ follows an inverse trend: δ decreases as CMF increases to 0.1 %, after which it rises again at 0.2 %. These results suggest that an optimal CMF content of around 0.1 % provides the best combination of sensitivity and

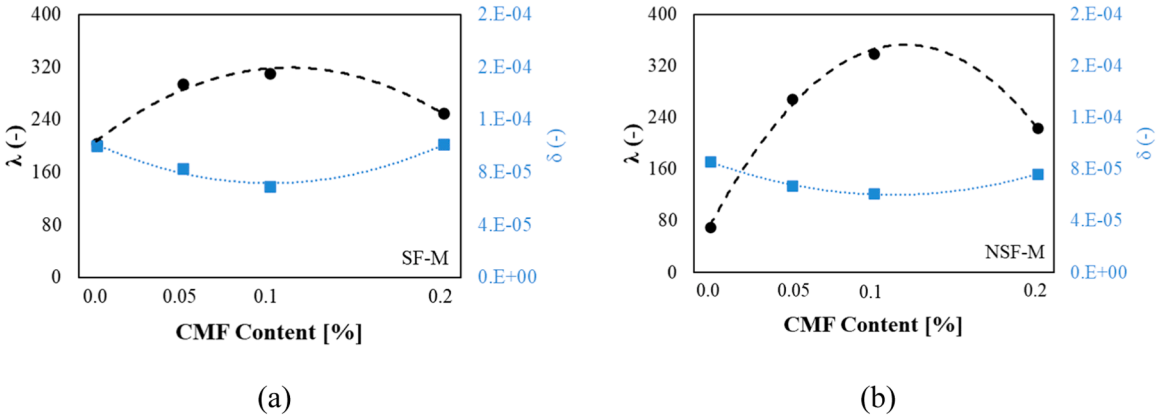

Fig. 9. Results of electrotechnical testing for mixes: (a) SF-M; (b) NSF-M.

linearity for piezoresistive sensing.

Compared to the baseline SF-M mix with 0 % CMF, the addition of 0.05, 0.1, and 0.2 % CMF results in increases in λ by approximately 1.5, 1.5, and 1.2 times, respectively. For the NSF-M specimens, the exact CMF dosages result in even greater improvements: 3.8, 4.8, and 3.2 times, respectively. This indicates that incorporating CMF significantly enhances piezoresistive sensitivity, particularly in the NSF-M, which lacks silica fume [25]. The larger relative improvement in NSF-M suggests that CMFs play a more dominant role in forming conductive pathways when the matrix is less refined. In contrast, the denser microstructure of SF-M (owing to silica fume) already offers improved conductivity, thus diminishing the relative impact of CMF addition. These findings highlight a synergistic but non-additive interaction between matrix composition and fibre content. While CMFs improve the sensing response in both cases, their effectiveness is more pronounced in a coarser matrix (e.g., NSF-M), where conductive network formation is otherwise limited [7,41,44].

The results also suggest that silica fume has a stabilising effect on gauge factor variability. In SF-M mixes, changes in λ with increasing CMF content are less dramatic than in NSF-M, indicating a more stable electromechanical response. This may be attributed to silica fume's role in refining the matrix and enhancing the fibre-matrix interfacial bond, which facilitates more uniform stress transfer during loading [45,46]. Additionally, a particularly interesting finding is that the mortar containing silica fume exhibited a notably high gauge factor even in the absence of CMF. This behaviour is likely explained by the presence of shrinkage-induced microcracks, which tend to close under compressive loading, thereby increasing electrical conductivity and contributing to the elevated gauge factor. Nevertheless, the sensing linearity (δ) shows no substantial difference between SF-M and NSF-M at equivalent CMF contents, implying that while silica fume improves piezoresistive sensitivity (λ), it does not significantly affect the linearity of the resistivity-strain relationship.

4. Conclusions

This study examined the combined effects of carbon microfibers (CMF) and silica fume on the mechanical and electrical properties of hydraulic lime-based mortars and pastes. Four mix types were developed: SF-M and SF-P (mortar and paste containing silica fume), and NSF-M and NSF-P (mortar and paste without silica fume). Each mix was reinforced with CMF at varying contents of 0 %, 0.05 %, 0.1 %, and 0.2 %. From the experimental results, the following conclusions were drawn:

- The inclusion of silica fume enhanced the compressive strength of hydraulic lime-based mortars and pastes due to its pozzolanic activity and the refinement of pore structure. However, it decreased flexural strength compared to the mixes without silica fume (NSF-M and NSF-P), likely due to increased brittleness and autogenous shrinkage, which can lead to micro-cracking.
- The addition of CMFs exhibited a nonlinear trend in mechanical performance. Increasing the CMF content up to 0.1 % resulted in a reduction in both compressive and flexural strengths, probably due to poor fibre dispersion and increased porosity. However, beyond 0.1 %, the strength improved, likely due to better fibre-matrix interaction and crack-bridging effects as the fibre dispersion became more effective.
- Electrical resistivity increased with curing time across all mixes. For mortars (SF-M and NSF-M), resistivity rose sharply between 7 and 28 days and then increased more slowly up to 60 days, reflecting matrix densification and continued hydration. In pastes (SF-P and NSF-P), resistivity increased more gradually, likely due to finer pore structures and the absence of aggregates, which help enhance conduction continuity.
- At 28 and 60 days, the mixes containing 0.1 % CMF demonstrated the lowest electrical resistivity, indicating the most effective formation of conductive networks. This trend was consistent with piezoresistivity results, where 0.1 % CMF produced the highest gauge factor (λ) and the lowest sensing linearity (δ), identifying it as the optimal fibre content for sensing performance.
- Both mechanical and microstructural characteristics influenced piezoresistive behaviour. While silica fume improved compressive strength and matrix density, it also modified the CMF network refining the pore structure in SF-M mixes. This refinement decreased ionic conduction pathways and resulted in a more stable response but slightly reduced sensitivity, leading to lower gauge factors compared to NSF-M mixes. Conversely, the more porous NSF-M mix allowed for greater fibre interconnection and higher gauge factors, although at the expense of reduced mechanical strength and stability. The nonlinearities observed in mechanical properties were reflected in piezoresistive responses, emphasising the importance of fibre distribution and matrix integrity. Optimal self-sensing performance was achieved through a balance between matrix refinement and the formation of a conductive fibre network.

This study was limited to a single CMF fibre length and short-term ageing (up to 60 days), without direct microstructural analyses such as SEM and element analysis (EDS). Future research should investigate the effects of CMF fibre length and aspect ratio, the long-term durability and sensing performance of the developed mortars under various environmental conditions and incorporate microstructural characterisation to better validate the observed mechanisms.

CRediT authorship contribution statement

Anastasios Drougkas: Writing – review & editing, Methodology. **Virginia Mendizabal:** Writing – review & editing, Investigation. **Ali Dalalbashi:** Writing – review & editing, Writing – original draft, Methodology, Investigation, Formal analysis, Data curation, Conceptualization. **Vasilis Sarhosis:** Writing – review & editing.

Declaration of Competing Interest

The authors declare that they have no known competing financial interests or personal relationships that could have appeared to influence the work reported in this paper.

Acknowledgements

The first author gratefully acknowledges support from UK Research and Innovation (UKRI) through the UK Government's Horizon Europe Guarantee (grant number EP/Z001641/1), provided under a Marie Skłodowska-Curie Postdoctoral Fellowship.

Appendix

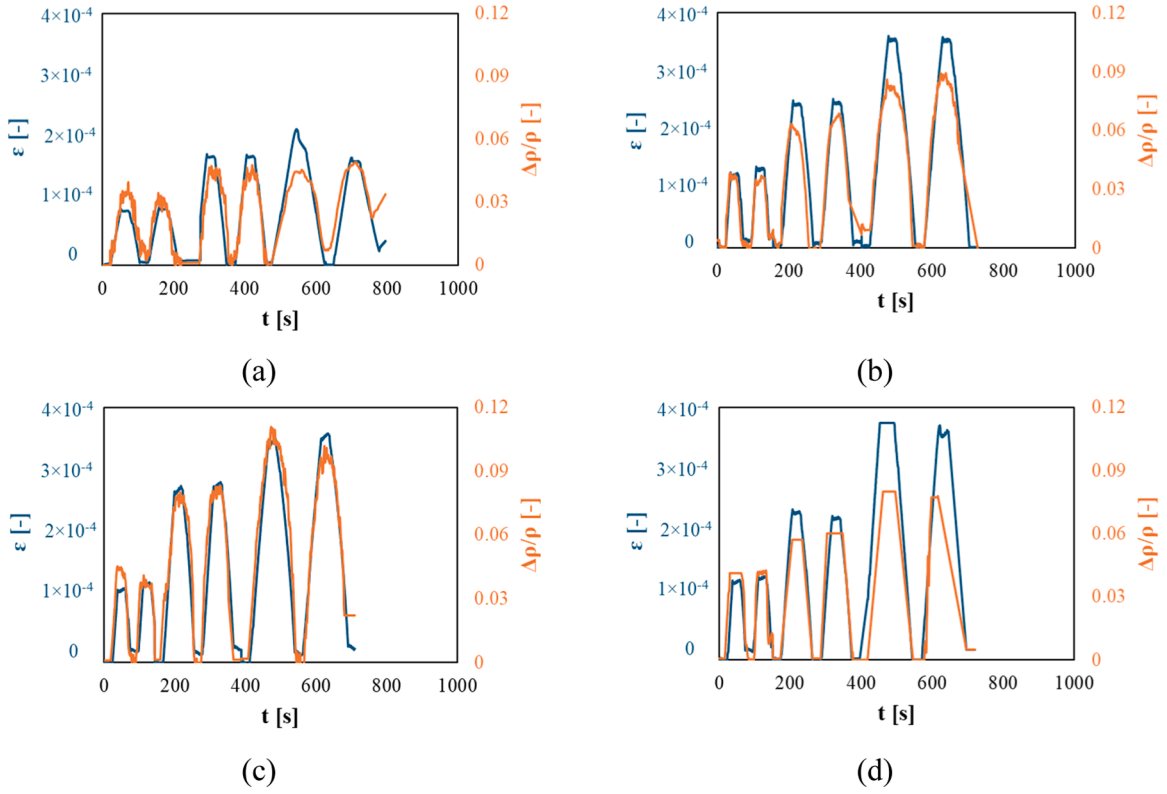

Fig.AP. 1. Time histories of axial strain (ε) and relative change in resistivity (Δρ/ρ) of mixes (a) SF-M-0; (b) SF-M-0.05; (c) SF-M-0.1; (d) SF-M-0.2

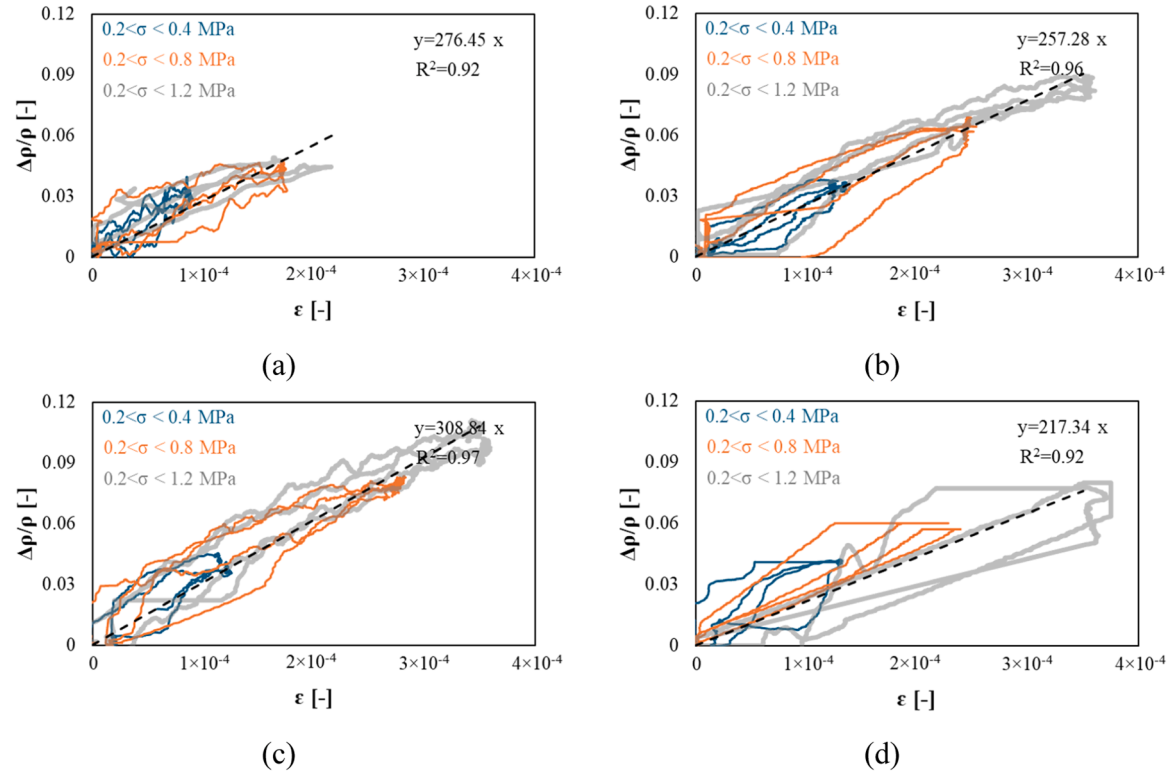

Fig.AP. 2. Correlation between axial strain and relative resistivity change at varying compressive stress ranges: (a) SF-M-0; (b) SF-M-0.05; (c) SF-M-0.1; (d) SF-M-0.2

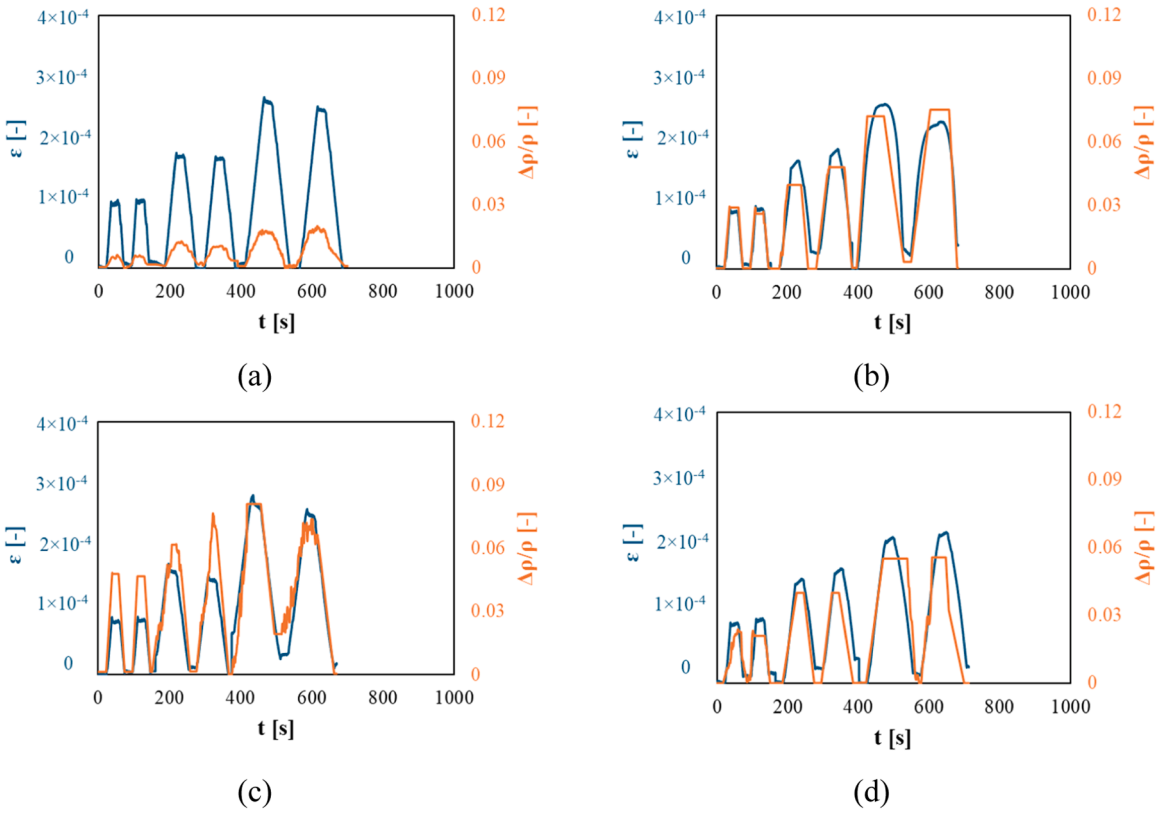

Fig.AP. 3. Time histories of axial strain (ε) and relative change in resistivity (Δρ/ρ) of mixes (a) NSF-M-0; (b) NSF-M-0.05; (c) NSF-M-0.1; (d) NSF-M-0.2

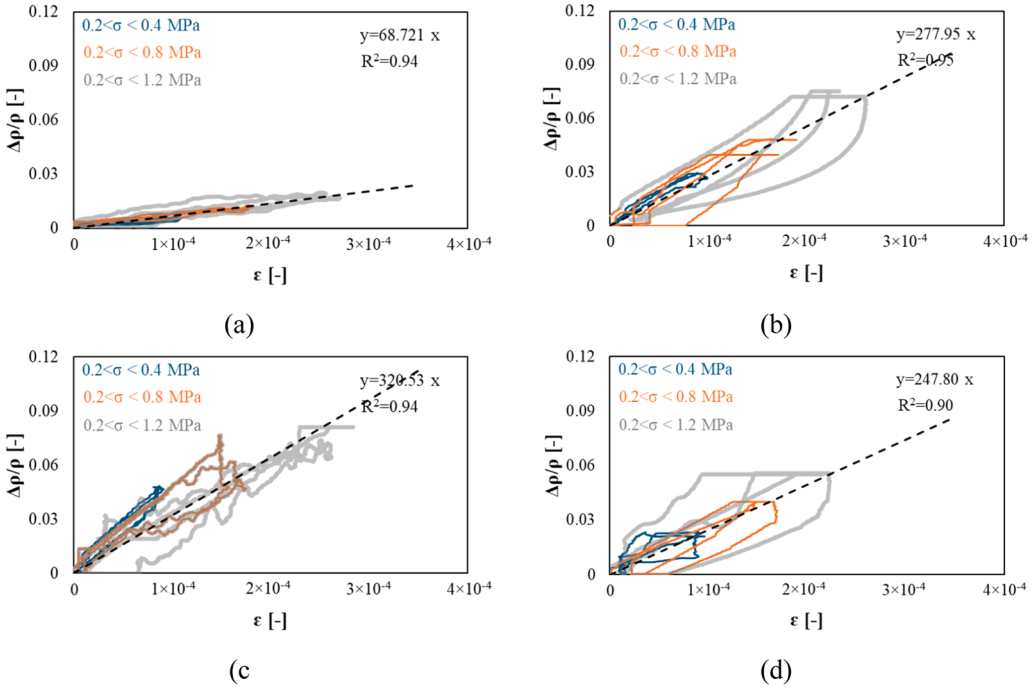

Fig.AP. 4. Correlation between axial strain and relative resistivity change at varying compressive stress ranges: (a) NSF-M-0; (b) NSF-M-0.05; (c) NSF-M-0.1; (d) NSF-M-0.2

Data availability

No data was used for the research described in the article.

References

[1] A. D'Alessandro, M. Rallini, F. Ubertini, A.L. Materazzi, J.M. Kenny, Investigations on scalable fabrication procedures for self-sensing carbon nanotube cement-matrix composites for SHM applications, Cem. Concr. Compos. 65 (2016) 200–213, https://doi.org/10.1016/j.cemconcomp.2015.11.001.

[2] B. Han, S. Ding, X. Yu, Intrinsic self-sensing concrete and structures: a review, Measurement 59 (2015) 110–128, https://doi.org/10.1016/j.measurement.2014.09.048.

[3] B. Shi, X. Chen, Y. Lu, X. Wang, K. Yao, Q. Dong, Smart cement-based materials from resistance-based self-sensing to capacitance-based self-sensing: a comprehensive review, J. Build. Eng. (2025) 113093, https://doi.org/10.1016/j.jobe.2025.113093.

[4] G.M. Kim, B.J. Yang, G.U. Ryu, H.K. Lee, The electrically conductive carbon nanotube (CNT)/cement composites for accelerated curing and thermal cracking reduction, Compos. Struct. 158 (2016) 20–29, https://doi.org/10.1016/j.compstruct.2016.09.014.

[5] S. Ding, Y. Ruan, X. Yu, B. Han, Y.Q. Ni, Self-monitoring of smart concrete column incorporating CNT/NCB composite fillers modified cementitious sensors, Constr. Build. Mater. 201 (2019) 127–137, https://doi.org/10.1016/j.conbuildmat.2018.12.203.

[6] H.B. Birgin, A. D'alessandro, S. Laflamme, F. Ubertini, Hybrid carbon microfibers-graphite fillers for piezoresistive cementitious composites, Sensors 21 (2021) 1–13, https://doi.org/10.3390/s21020518.

[7] H.B. Birgin, A. D'Alessandro, F. Ubertini, A new smart sustainable earth-cement composite doped by carbon microfibers with self-sensing properties, Dev. Built Environ. 14 (2023), https://doi.org/10.1016/j.dibe.2023.100168.

[8] A.K. Thomoglou, M.G. Falara, M.E. Voutetaki, J.G. Fantidis, B.A. Tayeh, C. E. Chalioris, Electromechanical properties of multi-reinforced self-sensing cement-based mortar with MWCNTs, CFs, and PPs, Constr. Build. Mater. 400 (2023), https://doi.org/10.1016/j.conbuildmat.2023.132566.

[9] P. Alafogianni, I. Tragazikis, A. Balaskas, N.-M. Barkoula, Structural properties and damage detection capability of carbon nanotube modified mortars after Freeze-Thaw, Materials 12 (2019) 1747, https://doi.org/10.3390/ma12111747.

[10] S.C. Marçula, J.B.L.P. e Silva, C.T.O. e Silva, R.C.C. Lintz, L.A. Gachet, Analysis of electrical and mechanical properties of Self-Sensing cement composite with carbon microfiber, Mater. Res. 28 (2025), https://doi.org/10.1590/1980-5373-mr-2025-0031.

[11] J. Donnini, T. Bellezze, V. Corinaldesi, Mechanical, electrical and self-sensing properties of cementitious mortars containing short carbon fibers, J. Build. Eng. 20 (2018) 8–14, https://doi.org/10.1016/j.jobe.2018.06.011.

[12] A. Mobili, C. Giosuè, T. Bellezze, G.M. Revel, F. Tittarelli, Gasification char and used foundry sand as alternative fillers to graphene nanoplatelets for electrically conductive mortars with and without virgin/recycled carbon fibres, Appl. Sci. (Switz.) 11 (2021) 1–16, https://doi.org/10.3390/app11010050.

[13] A. Belli, A. Mobili, T. Bellezze, P.B. Cachim, F. Tittarelli, Commercial and recycled carbon-based fillers and fibers for self-sensing cement-based composites: comparison of mechanical strength, durability, and piezoresistive behavior, J. Build. Eng. 73 (2023), https://doi.org/10.1016/j.jobe.2023.106836.

[14] Z. Tian, Y. Li, J. Zheng, S. Wang, A state-of-the-art on self-sensing concrete: materials, fabrication and properties, Compos B Eng. 177 (2019) 107437, https://doi.org/10.1016/j.compositesb.2019.107437.

[15] J. Han, J. Pan, J. Cai, X. Li, A review on carbon-based self-sensing cementitious composites, Constr. Build. Mater. 265 (2020) 120764, https://doi.org/10.1016/j.conbuildmat.2020.120764.

[16] W. Dong, W. Li, Z. Tao, K. Wang, Piezoresistive properties of cement-based sensors: review and perspective, Constr. Build. Mater. 203 (2019) 146–163, https://doi.org/10.1016/j.conbuildmat.2019.01.081.

[17] Y. Zhao, J. Zhang, S. Qiang, H. Lu, J. Li, Effect of carbon fibers and graphite particles on mechanical properties and electrical conductivity of cement composite, J. Build. Eng. 94 (2024), https://doi.org/10.1016/j.jobe.2024.110036.

[18] S. Wen, D.D.L. Chung, The role of electronic and ionic conduction in the electrical conductivity of carbon fiber reinforced cement, Carbon N. Y 44 (2006) 2130–2138, https://doi.org/10.1016/j.carbon.2006.03.013.

[19] O. Galao, F.J. Baeza, E. Zornoza, P. Garcés, Strain and damage sensing properties on multifunctional cement composites with CNF admixture, Cem. Concr. Compos 46 (2014) 90–98, https://doi.org/10.1016/j.cemconcomp.2013.11.009.

[20] X. Fu, D.D.L. Chung, Effect of curing age on the self-monitoring behavior of carbon fiber reinforced mortar, Cem. Concr. Res 27 (1997) 1313–1318, https://doi.org/10.1016/S0008-8846(97)00118-X.

[21] A.O. Monteiro, A. Loredo, P.M.F.J. Costa, M. Oeser, P.B. Cachim, A pressure-sensitive carbon black cement composite for traffic monitoring, Constr. Build. Mater. 154 (2017) 1079–1086, https://doi.org/10.1016/j.conbuildmat.2017.08.053.

[22] A.C. Mpalaskas, T.E. Matikas, D.G. Aggelis, Acoustic monitoring for the evaluation of concrete structures and materials, Acoust. Emiss. Relat. NonDestr. Eval. Tech. Fract. Mech. Concr. Fundam. Appl. (2021) 257–280, https://doi.org/10.1016/B978-0-12-822136-5.00013-7.

[23] M.C. Naoum, N.A. Papadopoulos, M.E. Voutetaki, C.E. Chalioris, Structural health monitoring of Fiber-Reinforced concrete prisms with polyolefin Macro-Fibers using a piezoelectric materials network under various Load-Induced stress, Buildings 13 (2023) 2465, https://doi.org/10.3390/buildings13102465.

[24] A.E. Dimou, C.M. Charalampidou, Z.S. Metaxa, S.K. Kourkoulis, I. Karatasios, G. Asimakopoulos, et al., Mechanical and electrical properties of hydraulic lime pastes reinforced with carbon nanomaterials, Procedia Struct. Integr. 28 (2020) 1694–1701, https://doi.org/10.1016/J.PROSTR.2020.10.144.

[25] A. Drougkas, V. Sarhosis, M. Basheer, A. D'Alessandro, F. Ubertini, Design of a smart lime mortar with conductive micro and nano fillers for structural health monitoring, Constr. Build. Mater. 367 (2023) 130024, https://doi.org/10.1016/j.conbuildmat.2022.130024.

[26] A. Drougkas, V. Sarhosis, A. Macente, M. Basheer, A. D'Alessandro, F. Ubertini, Mechanical and durability testing and XCT imaging of a Lime-Based Micro-Scale modified smart intervention mortar, Int. J. Archit. Herit. (2023) 1–16, https://doi.org/10.1080/15583058.2023.2278067.

[27] G. Allen, R. Ball, Mechanical properties of hydraulic lime mortars, 4th Port. Congr. Mortars ETICS (2012).

[28] A. El-Turki, R.J. Ball, S. Holmes, W.J. Allen, G.C. Allen, Environmental cycling and laboratory testing to evaluate the significance of moisture control for lime mortars, Constr. Build. Mater. 24 (2010) 1392–1397, https://doi.org/10.1016/j.conbuildmat.2010.01.019.

[29] S. Barr, W.J. McCarter, B. Suryanto, Bond-strength performance of hydraulic lime and natural cement mortared sandstone masonry, Constr. Build. Mater. 84 (2015) 128–135, https://doi.org/10.1016/j.conbuildmat.2015.03.016.

[30] V. Pavlík, M. Uzáková, Effect of curing conditions on the properties of lime, lime–metakaolin and lime–zeolite mortars, Constr. Build. Mater. 102 (2016) 14–25, https://doi.org/10.1016/j.conbuildmat.2015.10.128.

[31] J. Lanas, J.L. Perez Bernal, M.A. Bello, J.I. Alvarez, Mechanical properties of masonry repair dolomitic lime-based mortars, Cem. Concr. Res 36 (2006) 951–960, https://doi.org/10.1016/j.cemconres.2005.10.004.

[32] W. Chuang, J. Geng-sheng, L. Bing-liang, P. Lei, F. Ying, G. Ni, et al., Dispersion of carbon fibers and conductivity of carbon fiber-reinforced cement-based composites, Ceram. Int. 43 (2017) 15122–15132, https://doi.org/10.1016/J.CERAMINT.2017.08.041.

[33] BS EN 459-1, 2010, Building lime Part1: Definitions, specifications and conformity criteria.

[34] BS EN 13263-1, 2005, Silica fume for concrete: Definitions, requirements and conformity criteria.

[35] BS EN 196-1, 1995, Methods of testing cement: Determination of strength.

[36] BS EN 196-3, 2016, Methods of testing cement: Determination of setting times and soundness.

[37] W. Brameshuber (Ed.), RILEM TC 201-TRC: Textile reinforced concrete- state-of-the-art, RILEM, Bagneux, 2006.

[38] A. Peled, A. Bentur, B. Mobasher, Textile reinforced concrete, edition, 2017, CRC Press, August 9, 2017, p. 1.

[39] BS EN 1015-11, 1999, Methods of test for mortar for masonry. Determination of flexural and compressive strength of hardened mortar.

[40] D. Zhang, J. Zhao, D. Wang, Y. Wang, X. Ma, Influence of pozzolanic materials on the properties of natural hydraulic lime based mortars, Constr. Build. Mater. 244 (2020), https://doi.org/10.1016/j.conbuildmat.2020.118360.

[41] I. Kanellopoulou, I.A. Kartsonakis, A.I. Chrysanthopoulou, C.A. Charitidis, The effect of carbon nanotubes and carbon microfibers on the piezoresistive and mechanical properties of mortar, Fibers 12 (2024), https://doi.org/10.3390/fib12080062.

[42] G. Cosoli, A. Mobili, F. Tittarelli, G.M. Revel, P. Chiariotti, Electrical resistivity and electrical impedance measurement in mortar and concrete elements: a systematic review, Appl. Sci. 10 (2020) 9152, https://doi.org/10.3390/app10249152.

[43] M.M. Badalyan, N.G. Muradyan, R.S. Shainova, A.A. Arzumanyan, M. A. Kalantaryan, R.R. Sukiasyan, et al., Effect of silica fume concentration and Water-Cement ratio on the compressive strength of Cement-Based mortars, Buildings 14 (2024) 757, https://doi.org/10.3390/buildings14030757.

[44] A. D'Alessandro, F. Ubertini, Mechanical and durability investigation of composite mortar with carbon microfibers (CMF), Appl. Sci. 14 (2024), https://doi.org/10.3390/app14072773.

[45] Z.G. Liu, L.R. Yang, J.C. Wei, B.H. Zhao, X.X. Feng, Piezoresistive properties of cement mortar with carbon nanotube, 286, Adv. Mat. Res 284 (2011) 310, https://doi.org/10.4028/www.scientific.net/AMR.284-286.310.

[46] W. Yin, X. Li, T. Sun, Y. Chen, Z. Yu, M. Xu, Force-electric characteristics of cement-based materials with silica fume and Fly ash during uniaxial compression, J. Mater. Res. Technol. 24 (2023) 290–302, https://doi.org/10.1016/j.jmrt.2023.02.170.